Chinese Journal of
POLYMER SCIENCE

RESEARCH ARTICLE

https://doi.org/10.1007/s10118-026-3853-9
Chinese J. Polym. Sci.

Main-chain/Side-chain Synergistic Thermally Activated Delayed Fluorescence Conjugated Polymers for White Organic Light-emitting Diodes

Ming-Xiao Liu[a], Kai Jiang[c], Shao-Kui Cao[b], Zheng-Hao Zhao[a], Ming-Liang Zhao[a], Kun-Lun Wang[a], Ying-Liang Liu[a], Er-Gang Wang[d], Shi-Jian Su[b*], and Shen-Gang Xu[a*]

[a] *School of Materials Science and Engineering, Henan Key Laboratory of Advanced Nylon Materials and Application, Zhengzhou University, Zhengzhou 450001, China*
[b] *Zhengzhou Key Laboratory of Organic Optoelectronics, Faculty of Engineering, Huanghe Science & Technology University, Zhengzhou 450061, China*
[c] *State Key Laboratory of Luminescent Materials and Devices and Institute of Polymer Optoelectronic Materials and Devices, South China University of Technology, Guangzhou 510640, China*
[d] *Department of Chemistry and Chemical Engineering, Chalmers University of Technology, Göteborg SE-412 96, Sweden*

Electronic Supplementary Information

Abstract Existing strategies for single-molecule white light-emitting polymers, either embedding light-emitting units into the conjugated main chain or attaching them to a non-conjugated main chain, cannot simultaneously achieve efficient charge transport and high-quality white light emission. In this study, a series of conjugated polymers, PCFDF-DT-DN$_x$ (x=0, 0.25, 0.5, 1.5, 2.5, 5, or 10), bearing thermally activated delayed fluorescence (TADF) green-emitting units in the main chain and red-emitting units in the side chain were designed and synthesized. The conjugated backbone containing green units was synthesized *via* Suzuki polymerization, whereas the red TADF units were attached to the backbone *via* a post-click reaction. The main-chain/side-chain synergistic effect enables PCFDF-DT-DN$_x$ to exhibit good charge-transporting ability and facile emission color tunability. The non-doped device using PCFDF-DT-DN$_{10}$ as the emissive layer (EML) exhibited near-warm white light with CIE coordinates of (0.41, 0.49), a maximum external quantum efficiency (EQE$_{max}$) of 1.58%, and a maximum luminance (L_{max}) of 3169.2 cd·m^{-2}. The doped device based on PCFDF-DT-DN$_{10}$ 10 wt% in CBP achieved cool white light with CIE coordinates of (0.31, 0.42), an EQE$_{max}$ of 3.96%, and a L_{max} of 4050.9 cd·m^{-2}. This strategy validates the feasibility of the design and offers a new route toward high-efficiency white-light-emitting polymers with a facile synthesis and tunable emission colors.

Keywords Organic light-emitting diode (OLED); Thermally activated delayed fluorescence (TADF); Single-molecule white light-emitting polymer (SMWLEP); Conjugated polymer; Main-chain/side-chain synergy

Citation: Liu, M. X.; Jiang, K.; Cao, S. K.; Zhao, Z. H.; Zhao, M. L.; Wang, K. L.; Liu, Y. L.; Wang, E. G.; Su, S. J.; Xu, S. G. Main-chain/side-chain synergistic thermally activated delayed fluorescence conjugated polymers for white organic light-emitting diodes. *Chinese J. Polym. Sci.* https://doi.org/10.1007/s10118-026-3853-9

INTRODUCTION

White organic light-emitting diodes (WOLEDs) have broad application prospects in the fields of display and lighting owing to their surface light source characteristics, high color rendering index (CRI), and flexibility.[1–3] Thermally activated delayed fluorescence (TADF) materials featuring an extremely small singlet-triplet energy gap (ΔE_{ST}) can achieve 100% exciton utilization through the reverse intersystem crossing (RISC) process. Moreover, they contain no noble metals and their emission colors are easy to regulate, making them an ideal material system for constructing high-efficiency WOLEDs.[4–10] However, the synergistic improvement of device luminance, efficiency, and stability, while reducing preparation costs for large-scale manufacturing, remains a key scientific and technological problem to be solved urgently in this field.[11]

To achieve white-light emission, it is common to combine red, green, and blue primary-color emitting units, or a pair of complementary color-emitting units (*e.g.*, blue/yellow), to obtain continuous broad-spectrum emission through incomplete energy transfer.[12–14] Traditional multi-emissive-layer structures and small-molecule blending systems impose stringent requirements on the component ratio, energy level matching, and energy transfer processes.[15–18] Meanwhile, they are prone to phase separation, crystallization, and poor film stability. In addition, these systems rely heavily on vacuum evaporation, which does not meet the demand for low-

* Corresponding authors, E-mail: mssjsu@scut.edu.cn (S.J.S.)
E-mail: xusg@zzu.edu.cn (S.G.X.)
Received July 8, 2026; Accepted August 17, 2026; Published online November 4, 2026

© Chinese Chemical Society
Institute of Chemistry, Chinese Academy of Sciences

cost and large-area fabrication.[19–21] Benefiting from their good solubility, excellent film-forming ability, and effective suppression of phase separation, single-molecule luminescent polymers have become promising candidates for constructing solution-processed high-efficiency and stable WOLEDs.[11,22]

Existing strategies for the molecular design of single-molecule white light-emitting polymers (SMWLEPs) are mainly divided into two types. The first strategy is to covalently embed short-wavelength (SW) and long-wavelength (LW) TADF units into a conjugated main chain (Chart 1a), using incomplete energy transfer to achieve white-light emission. For example, Wang *et al*.[23] embedded red and green TADF units into a blue fluorescent polycarbazole main chain to obtain a conjugated polymer PCzTx-Q*x* that integrates blue, green, and red emissions. The device fabricated with PCzTx-Q0.1 as the emitting layer achieved warm white light with CIE coordinates of (0.55, 0.39) and a high maximum external quantum efficiency (EQE_{max}) of 23.9%, fully demonstrating the advantage of the conjugated backbone in charge transport. However, multi-monomer copolymerization also leads to the complex synthesis of monomers and low reproducibility of the polymers. The second strategy is to attach TADF units of different wavelengths to the non-conjugated side chains (Chart 1b). In our recent work,[24] blue DT and orange-red TB units were attached to a non-conjugated main chain at different ratios. This strategy significantly improved the solubility and side-chain design flexibility, and P3 successfully achieved white-light emission with CIE coordinates of (0.33, 0.40). Nevertheless, the non-conjugated main chain structure weakens the charge transport to some extent, resulting in relatively high turn-on voltages (4.6–6.6 V) and low luminance (110–374 cd·m^{-2}) for this series of devices. Collectively, the former strategy offers excellent charge transport but suffers from complex synthesis, poor solubility, and reproducibility, whereas the latter provides flexible tunability but has insufficient charge transport ability.

To address this contradiction, our group recently proposed a new strategy that combines the advantages of both approaches (Chart 1c). A conjugated main chain was used to ensure charge transport, while red- and green-emitting units were flexibly attached to the side chains for color tuning.[25] Based on this strategy, PCFTN-*X*, a TADF polymer, was synthesized. Non-doped device D3 fabricated with PCFTN-3 as the emitting layer exhibited excellent device performance. Its turn-on voltage (V_{on}) was only 3.4 V, with an EQE_{max} of 10.23%, a current efficiency (CE_{max}) of 20.14 cd·A^{-1}, and a maximum luminance (L_{max}) of 3264 cd·m^{-2}. Stable white-light emission with CIE coordinates of (0.34, 0.38) was achieved. This verified the feasibility of the proposed strategy.

Inspired by this, the present study attempted to further optimize the molecular structure of SMWLEP (Chart 1d). Because white-light emission requires a relatively high content of SW units, unlike the previous strategy where both red- and green-emitting units were attached to side chains, the SW green units DT were first embedded into the conjugated main chain *via* Suzuki polycondensation. This approach effectively maintains the long-range conjugated structure of the polymer, further improving the hole and electron mobilities, which contributes to a reduction in the driving voltage. It also avoids aggregation-caused quenching (ACQ) resulting from high-density side-chain attachment, thereby achieving stable green emission. Meanwhile, the LW red units DN are attached to the side chain *via* a post-click reaction. To further balance the emission color and enhance the hole transport ability, an additional compound, mCP-Alkyne, which possesses both blue fluorescence and hole transport functions, was introduced into the side chains. This enables precise and reg-

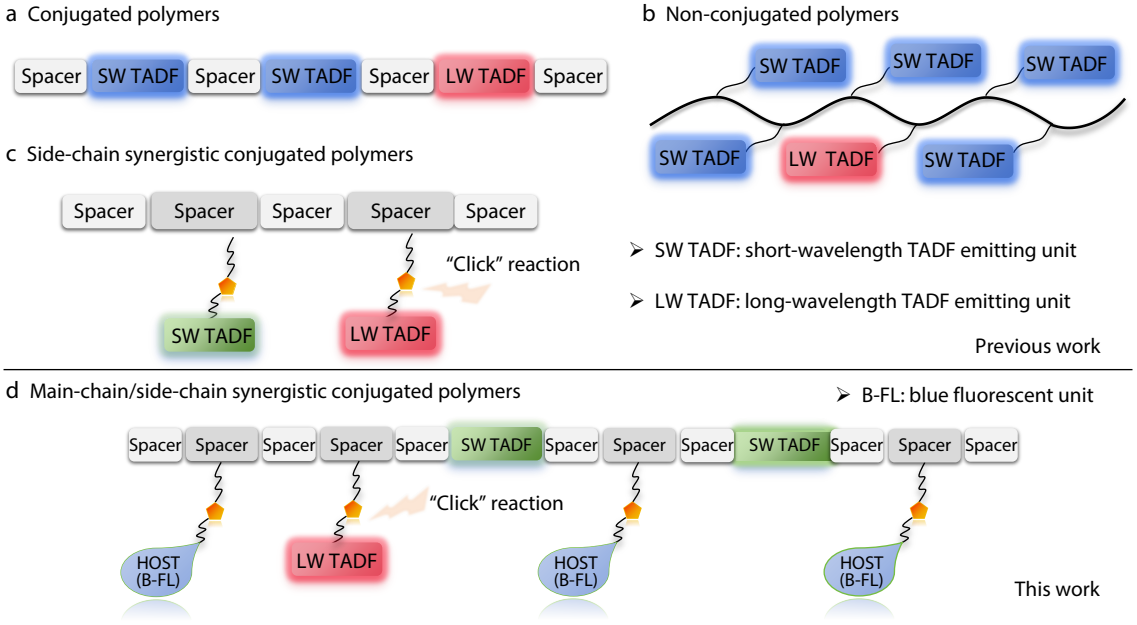


Chart 1 Structural schematic diagrams of single-molecule white light-emitting polymers: (a) conjugated polymers, (b) non-conjugated polymers, (c) side-chain synergistic conjugated polymers, and (d) main-chain/side-chain synergistic conjugated polymers.

https://doi.org/10.1007/s10118-026-3853-9

ular tuning of the emission color. Based on this design, a series of "main-chain/side-chain synergistic" TADF-conjugated polymers, named PCFDF-DT-DN$_x$ (x=0, 0.25, 0.5, 1.5, 2.5, 5, or 10) were synthesized. Using PCFDF-DT-DN$_x$ as the emitting layer, both non-doped and doped organic light-emitting diode (OLED) devices were successfully fabricated *via* the spin-coating method. The non-doped OLED device based on PCFDF-DT-DN$_{10}$ achieved near-warm white light emission with CIE coordinates of (0.41, 0.49), CRI of 88.9, V_{on} of 3.3 V, L_{max} of 3169.2 cd·m^{-2}, and EQE$_{max}$ of 1.58%. In addition, a doped OLED device based on the PCFDF-DT-DN$_{10}$ 10 wt% in 4,4′-bis(9*H*-carbazol-9-yl)biphenyl (CBP) achieved cool white emission with CIE coordinates of (0.31, 0.42). Its EQE$_{max}$ is 3.96%, and L_{max} reaches 4050.9 cd·m^{-2}, showing a significantly improved overall device performance. This design overcomes both the difficulties in composition control and solubility of conjugated main-chain polymers caused by multi-monomer copolymerization and the deficiency in charge transport of non-conjugated side-chain polymers, while achieving broadband emission tuning. The resulting polymers exhibited good thermal stability and solution processability, confirming the feasibility of this strategy and offering a new design concept for high-performance, solution-processed WOLEDs.

EXPERIMENTAL

Materials

All chemical reagents were purchased from commercial sources and used without further purification, unless otherwise specified. The organic solvents required for the chemical synthesis were purified using standard methods prior to use.

Synthesis

As illustrated in Scheme 1, the green TADF functional compound DT-Br was used as the dibrominated functional monomer.[25] The equimolar DT-Br and 3,6-dibromocarbazole (3,6-Cz-Br) were copolymerized with the fluorene-based diboronate monomer F-BO *via* Suzuki polycondensation to afford the precursor polymer backbone PCFDF-Br. Subsequent azidation of PCFDF-Br yielded the azide-functionalized conjugated backbone PCFDF-N$_3$. Furthermore, according to our previous work, the alkynyl-terminated red TADF functional compound DN-Alkyne and the host functional compound mCP-Alkyne were synthesized. The synthetic procedures for PCFDF-N$_3$, DT-Br, DN-Alkyne, and mCP-Alkyne are depicted in Schemes S1–S4 (in the electronic supplementary information, ESI), respectively.

Synthesis of target polymers PCFDF-DT-DN$_x$ (x=0, 0.25, 0.5, 1.5, 2.5, 5 or 10). As outlined in Scheme 1, the target polymers were synthesized *via* a sequential azide-Alkyne click reaction between PCFDF-N$_3$ and the functionalized compounds DN-Alkyne and mCP-Alkyne. Specifically, DN-Alkyne was first introduced; upon its complete consumption, mCP-Alkyne was subsequently added. The progress of the reaction was monitored using thin-layer chromatography (TLC). The molar ratio of DN-Alkyne to mCP-Alkyne was fixed at x/(50 − x), and the resulting polymers were designated as PCFDF-DT-DN$_x$ (x=0, 0.25, 0.5, 1.5, 2.5, 5, or 10), where x denotes the molar percentage of the DN-Alkyne relative to the total alkynyl-functionalized compounds employed. To ensure full conversion of the azido groups in PCFDF-N$_3$, the azide-to-Alkyne molar ratio was maintained at 1:1.5, corresponding to a 50% excess of the mCP-Alkyne. Upon completion of the reaction, 1,4,7,10-tetraazacyclododecane was introduced to chelate and remove residual copper ions. The crude products were subsequently purified by sequential Soxhlet extraction using methanol and diethyl ether for 36 h each. The final products were obtained as yellow-green solid powders in isolated yields ranging from 56% to 59%. The detailed synthetic procedures and characterization data are provided in ESI.

Instrumentation

^{1}H nuclear magnetic resonance (^{1}H-NMR) spectroscopy, electrospray ionization mass spectrometry (ESI-MS), Fourier transform infrared (FTIR) spectroscopy, differential scanning calorimetry (DSC), thermogravimetric analysis (TGA), X-ray diffraction (XRD), ultraviolet-visible (UV-Vis) absorption spectroscopy, and photoluminescence (PL) spectroscopy were used to characterize the chemical structures and photophysical properties of all intermediates, functional monomers, and target polymers. Cyclic voltammetry (CV) was used to measure electrochemical properties. Detailed information on the instrument parameters and experimental procedures is provided in ESI.

Device Fabrication and Measurement

The structure of the OLED device was as follows: ITO/PEDOT:PSS (40 nm)/PVK: Poly-TPD (mass ratio 4:1, 30 nm)/PCFDF-DT-DN$_x$ (20 nm)/TmPyPB (40 nm)/CsF (1.4 nm)/Al (50 nm). Detailed information on the device fabrication process and performance test methods is provided in ESI.

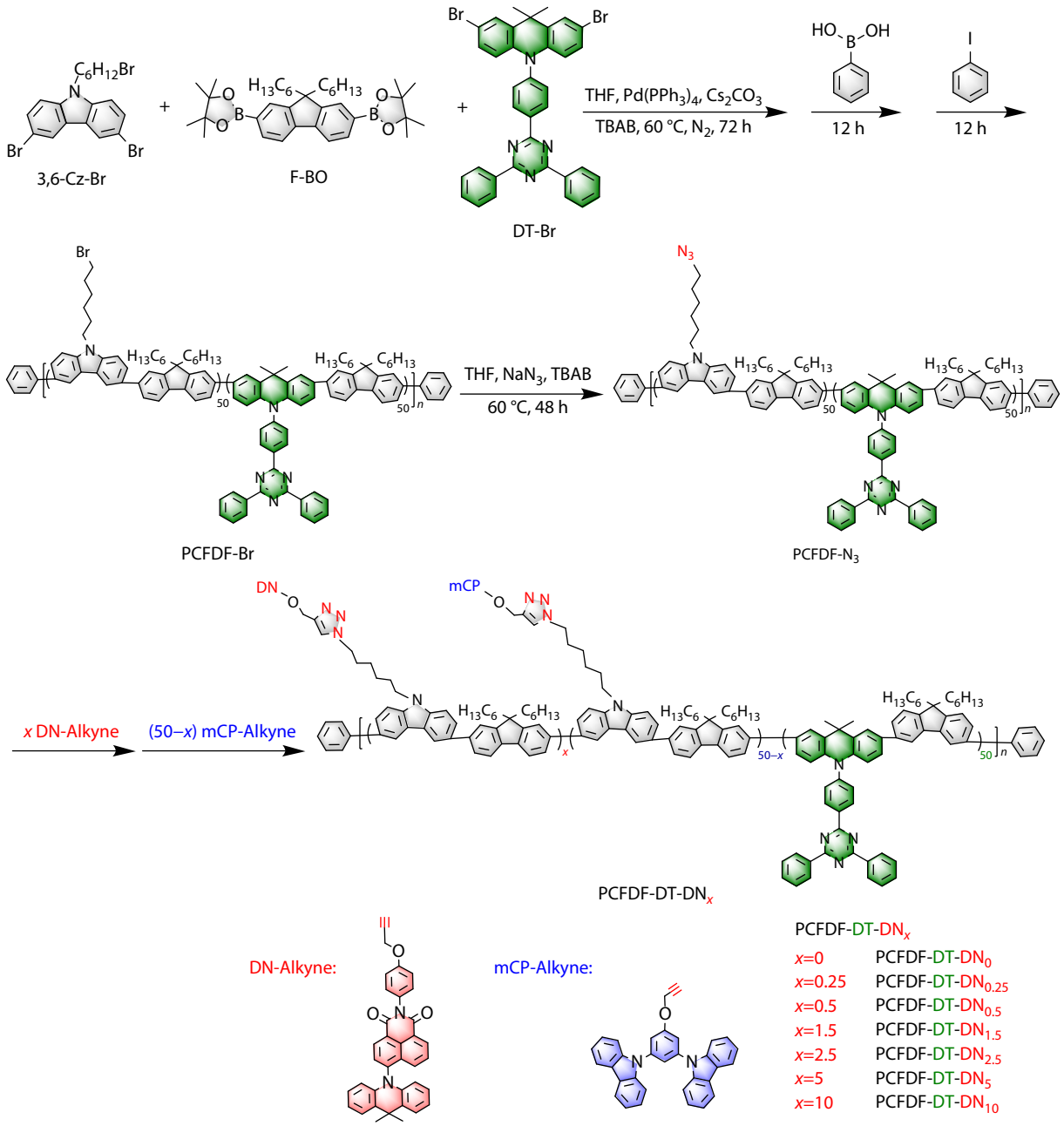
RESULTS AND DISCUSSION

Chemical Structures Characterization

Multiple characterization techniques, including ^{1}H-NMR, MALDI-TOF MS, ESI-MS, and FTIR, were employed to confirm the chemical structures of the intermediates, functional compounds, monomers, and target polymers.

Fig. 1 shows the comparison of ^{1}H-NMR spectra of mCP-Alkyne, DN-Alkyne, PCFDF-N$_3$, and PCFDF-DT-DN$_x$ in $CDCl_3$. The ^{1}H-NMR spectra of the other intermediates are shown in Figs. S1–S15 (in ESI). In the comparison of ^{1}H-NMR spectra among mCP-Alkyne, DN-Alkyne, PCFDF-N$_3$ and PCFDF-DT-DN$_{10}$ (Fig. 1A), the proton signal of the —CH_2— neighboring to azide group at 3.25 ppm and the alkyne proton signals at 4.80 and 2.61 ppm completely disappeared. Meanwhile, the characteristic proton peaks (a–e) attributed to mCP-Alkyne and DN-Alkyne appeared, providing direct and strong evidence for the successful click reaction. In Fig. 1(B), with increasing DN content in PCFDF-DT-DN$_x$, the proton peaks (b, c, d, and e) of the DN units gradually increased in intensity, despite being less prominent because of the lower content. The actual molar incorporation ratios of DN units to DT units in PCFDF-DT-DN$_x$ were determined by ^{1}H-NMR spectroscopy to be 2.70/50, 4.85/50, and 10.12/50 for x=2.5, 5, and 10, respectively, which closely matched the corresponding feed ratios of the DN-Alkyne and confirmed the efficient incorporation of DN units during the post-click reaction (the detailed calculation procedure is provided in ESI). This result confirms that the DN content in the polymers can be precisely tuned by varying the amount of DN-Alkyne added during synthesis.

https://doi.org/10.1007/s10118-026-3853-9



Scheme 1 Synthetic routes of polymer backbone PCFDF-N_3 and target polymers PCFDF-DT-DN_x (x=0, 0.25, 0.5, 1.5, 2.5, 5 or 10).

Further FTIR analysis (Figs. S21 and S22 in ESI) revealed the disappearance of the characteristic vibrational bands of the alkynyl (3297 and 2120 cm^{-1}) and azido (2092 cm^{-1}) groups in the spectra of PCFDF-DT-DN_x. Instead, a carbonyl stretching band at 1690 cm^{-1}, attributed to the DN unit, was observed. Gel permeation chromatography (GPC) was used to determine the molecular weights and molecular weight distributions of the polymer backbone and target polymers. Compared to the M_n of PCFDF-N_3 (6.39 kDa), the M_n values of PCFDF-DT-DN_5 and PCFDF-DT-DN_{10} in PCFDF-DT-DN_x exhibited a significant increase, being 8.91 and 8.82 kDa, respectively. This increase, along with the structural characterization results from ^{1}H-NMR and FTIR, confirms the successful click reaction and the effective attachment of functional units to the polymer backbone. (Fig. S24 and Table S1 in ESI).

Solubility, Crystallinity and Thermal Stability

To clarify the processing conditions for spin-coating of PCFDF-DT-DN_x, PCFDF-DT-DN_5 and PCFDF-DT-DN_{10} were selected as representative samples to test their solubility (concentration of 5 mg·mL^{-1}; see the digital photograph in Fig. S25 in ESI) in common organic solvents. PCFDF-DT-DN_x could dissolve in most common organic solvents such as dichloromethane (DCM) and tetrahydrofuran (THF). This excellent solubility is mainly attributed to the fluorene units in the polymer main chain and the hexyl groups introduced into the side chains. This solubility study not only provides a clear basis for the selection of solvents in the subsequent polymer purification process but, more

https://doi.org/10.1007/s10118-026-3853-9

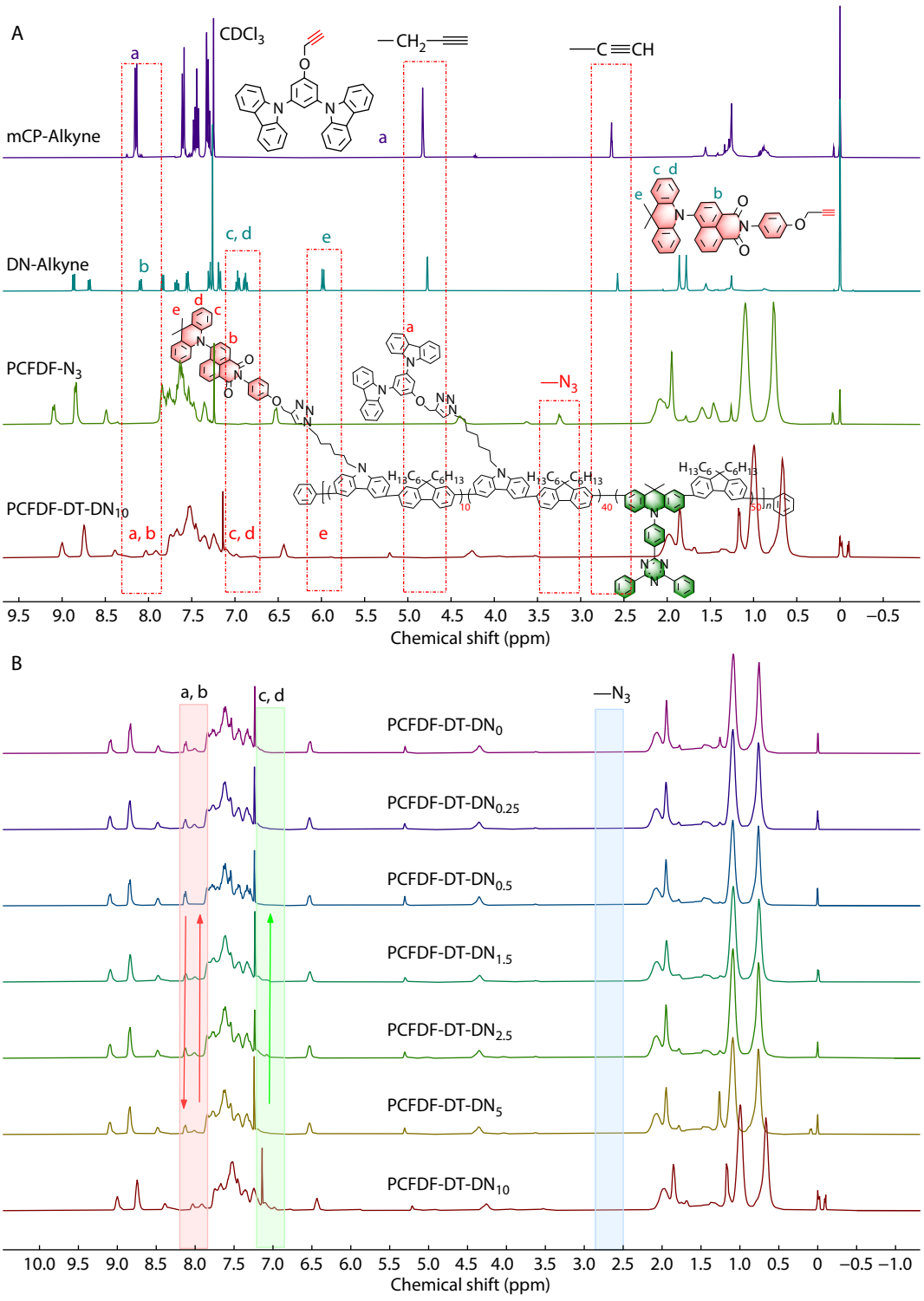


Fig. 1 ^{1}H-NMR spectra (chloroform-*d*) of (A) mCP-Alkyne, DN-Alkyne, PCFDF-N_3 and PCFDF-DT-DN_{10}; (B) PCFDF-DT-DN_x (x=0, 0.25, 0.5, 1.5, 2.5, 5 or 10).

importantly, ensures that a homogeneous and stable precursor solution can be obtained during polymer spin-coating film formation, laying a key technological foundation for the preparation of high-performance solution-processed WOLED devices.

In addition, the crystalline properties of PCFDF-DT-DN_x were analyzed using XRD. The XRD patterns of all the samples (Fig. S26 in ESI) exhibited typical amorphous characteristics, that is, only broad and diffused "bread-like" peaks were observed, without distinct crystalline diffraction peaks. The formation of this amorphous structure is mainly attributed to the random orientation of the polymer main chain and the steric hindrance effects caused by the side chains. This sug-

https://doi.org/10.1007/s10118-026-3853-9

gests that the attachment of the TADF chromophores to the polymer backbone may reduce their crystallization tendency. Benefiting from this structural feature, the polymers can achieve higher film uniformity and morphological stability during spin-coating film formation, thereby effectively suppressing phase separation and fluorescence quenching effects. This characteristic is crucial for optimizing the preparation process and improving the overall performance of WOLED devices.

Finally, the thermal stability of PCFDF-DT-DN$_x$ was tested using TGA and DSC, and the results are shown in Fig. 2 and summarized in Table 1. As shown in Fig. 2(a), under a nitrogen atmosphere with a heating rate of 10 °C·min^{-1}, all the polymers exhibited thermal decomposition temperatures (T_d) exceeding 350 °C. The glass transition temperature (T_g) increases from 203.3 °C for PCFDF-DT-DN$_0$ to 217.7 °C for PCFDF-DT-DN$_{10}$ with increasing content of DN units (Fig. 2b), reflecting the enhanced polymer rigidity imparted by the more rigid DN units. This indicates that PCFDF-DT-DN$_x$ possesses excellent thermal stability, which is beneficial for the fabrication of WOLEDs with high thermal stability.

Photophysical and Electrochemical Properties

Fig. 3 displays the UV-Vis absorption spectra of DT-Br, DN-Alkyne, mCP-Alkyne, PCFDF-N$_3$, and PCFDF-DT-DN$_x$ (x=0, 0.25, 0.5, 1.5, 2.5, 5, or 10) in chloroform solution and the solid thin-film state. As shown in Fig. 3(a), PCFDF-DT-DN$_x$ exhibited significant absorption peaks at 276, 338, and 369 nm in the chloroform solution. Compared with PCFDF-N$_3$, the absorption peaks at 276 and 338 nm are attributed to the π-π^* transitions of the carbazole groups in the polymer backbone, the mCP unit, and the acridine moiety of the DT unit, respectively. The peak at 369 nm was assigned to the n-π^* transition of the conjugated structure in the main chain.[26,27] In addition, owing to the large intermolecular distance in solution and the relatively low grafting ratio of the DN units, a weak absorption band from 420 nm to 575 nm was observed, which was attributed to the intramolecular charge transfer (ICT) from the donor acridine to the acceptor naphthalimide in the DN unit.[28,29] Notably, the inset (enlarged view) shows that as the DN content increases, the ICT absorption peak intensity at approximately 475 nm gradually increases, confirming that the red TADF units DN have been successfully grafted into the polymer backbone. According to the absorption edge of the UV-Vis spectra, the optical band gap E_g of PCFDF-DT-DN$_x$ was calculated to be in the range of 2.95–2.98 eV.[30,31] Fig. 3(b) shows the UV-Vis spectra of the polymer films. The overall absorption profiles are similar to those of the solution spectra. Notably, with increasing grafting ratio of DN units, the ICT absorption at 325–450 nm gradually increased in a regular trend, and this variation was much more pronounced in the film state. This behavior is closely related to molecular aggregation: tighter molecular packing in the solid film strengthens the electronic coupling and exciton interactions among chro-

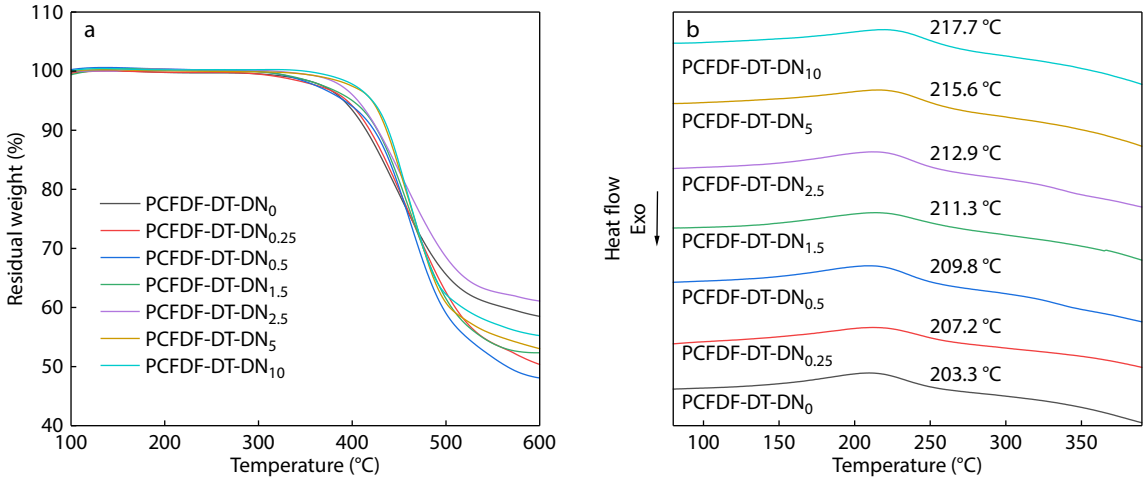


Fig. 2 (a) TG curves and (b) DSC curves of PCFDF-DT-DN$_x$ (x=0, 0.25, 0.5, 1.5, 2.5, 5 or 10).

Table 1 Thermal, photophysical and electrochemical properties of PCFDF-DT-DN$_x$ (x=0, 0.25, 0.5, 1.5, 2.5, 5 or 10).

PCFDF-DT-DN$_x$	T_d [a] (°C)	T_g [b] (°C)	λ_{abs} [c] (nm)	λ_{PL} [d] (nm)	PLQY [e] (%)	E_g [f] (eV)	HOMO [g] (eV)	LUMO [h] (eV)
PCFDF-DT-DN$_0$	399	203.3	273, 335, 365	522	8.97	2.98	−5.28	−2.30
PCFDF-DT-DN$_{0.25}$	404	207.2	275, 336, 367	526	9.46	2.98	−5.26	−2.28
PCFDF-DT-DN$_{0.5}$	396	209.8	274, 337, 368	526	9.57	2.98	−5.25	−2.27
PCFDF-DT-DN$_{1.5}$	408	211.3	275, 337, 366	523	8.74	2.98	−5.24	−2.26
PCFDF-DT-DN$_{2.5}$	410	212.9	276, 338, 369	522	7.81	2.98	−5.25	−2.27
PCFDF-DT-DN$_5$	428	215.6	278, 339, 372	529	9.36	2.97	−5.25	−2.28
PCFDF-DT-DN$_{10}$	427	217.7	279, 340, 373	546	7.31	2.98	−5.23	−2.25

[a] Decomposition temperature of 5% weight loss detected by TGA; [b] Glass transition temperature detected by DSC; [c] Maximum absorption wavelength in chloroform (0.1 mg·mL^{-1}); [d] Maximum emission wavelength in neat films; [e] Photoluminescence quantum yield in the thin-film state; [f] E_g estimated from the onset wavelengths (λ_{onset}) of the UV-Vis absorption spectra in chloroform (E_g = 1240/λ_{onset}); [g] HOMO energy levels estimated from the onset of the oxidation curves (E_{HOMO} = − (E_{OX} + 4.4)); [h] LUMO energy levels calculated by the equation of LUMO = HOMO + E_g.

https://doi.org/10.1007/s10118-026-3853-9

mophores. This phenomenon further confirms that the red TADF units have been quantitatively and successfully grafted onto the polymer side chains. This not only provides a prerequisite for efficient energy transfer between green and red TADF units but also offers a reliable photophysical basis for concentration-dependent emission tuning and broadband white-light emission.

In addition, the thin films of polymer backbone PCFDF-N_3 and target polymers PCFDF-DT-DN_x were irradiated under ultraviolet (UV) light (digital photos are shown in Fig. S23 in ESI). It can be clearly observed that with the increase of the proportion of red TADF units (*x* value) in the side chains, the emission color of the films gradually red-shifted from green to yellow-green. This phenomenon intuitively reflects the successful grafting of red TADF units (from absence to presence and from low to high content) and confirms the effective energy transfer from the host to the red-emitting guest. Meanwhile, compared with the polymer backbone PCFDF-N_3, all the target polymer films exhibited a significant increase in luminescence brightness. This result indicates that the introduction of mCP host units in the side chains can effectively improve the hole transport ability and exciton recombination efficiency of the films, thereby enhancing the luminescence brightness.[32] The above phenomena not only further confirm the success of the click chemistry modification, but also fully indicate that this series of polymer materials has great potential in the preparation of high-brightness, solution-processed WOLED devices.

Fig. 4 presents the PL spectra of the red and green TADF compounds (DT-Br and DN-Alkyne), mCP-Alkyne, PCFDF-N_3, and PCFDF-DT-DN_x in chloroform solution and thin films. As shown in Fig. 4(a), in solution, the emission peaks of DT-Br, DN-Alkyne, and mCP-Alkyne were mainly located at 530, 662, and 349 nm, respectively. For PCFDF-DT-DN_x, the PL emission peaks were mainly at 416 and 589 nm (λ_{exc}=350 nm). Compared with PCFDF-N_3 and DT-Br, the incorporation of DT into the polymer backbone resulted in a red shift of 59 nm for the DT emission, while the peak at 416 nm was attributed to the carbazole and fluorene moieties in the polymer backbone. By comparing the emission peaks of PCFDF-N_3, mCP-Alkyne, and PCFDF-DT-DN_0, it was found that after mCP was attached to the side chain, its emission peak red-shifted by approximately 67 nm, while the emission peak of PCFDF-N_3 also showed a slight red-shift and broadening. In addition, compared with PCFDF-DT-DN_0, the incorporation of DN units into the side chains led to a slight red shift and broadening of the emis-

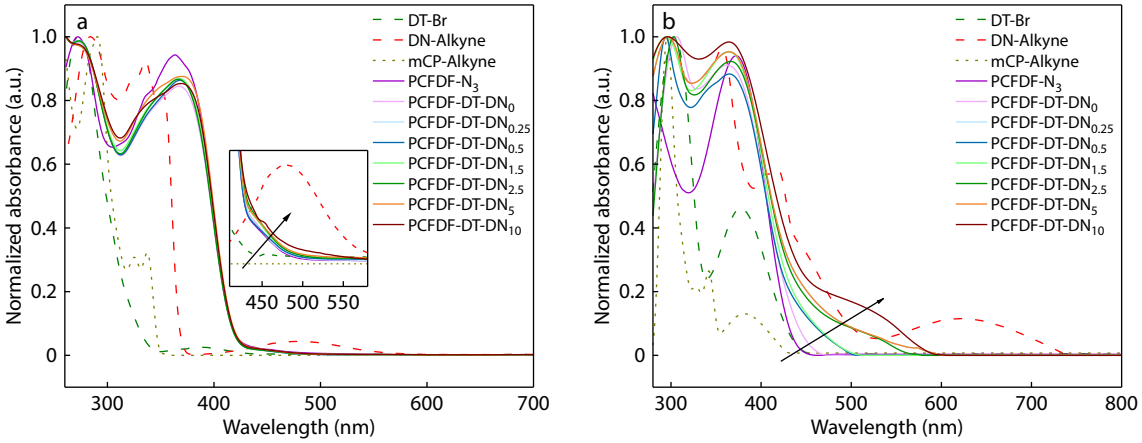


Fig. 3 UV-Vis absorption spectra of DT-Br, DN-Alkyne, mCP-Alkyne, PCFDF-N_3 and PCFDF-DT-DN_x (*x*=0, 0.25, 0.5, 1.5, 2.5, 5 or 10) in (a) chloroform solution and (b) film state.

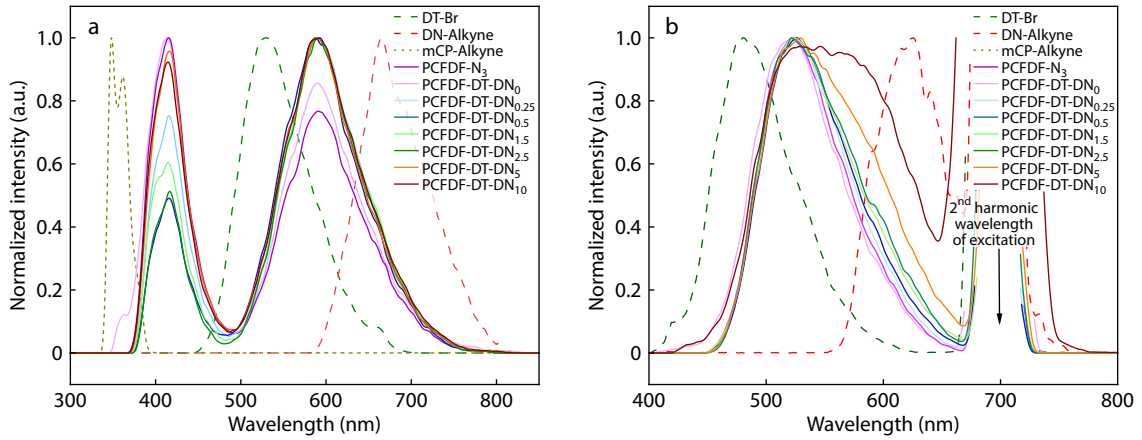


Fig. 4 PL spectra of DT-Br, DN-Alkyne, mCP-Alkyne, PCFDF-N_3 and PCFDF-DT-DN_x (*x*=0, 0.25, 0.5, 1.5, 2.5, 5 or 10) in (a) chloroform solution and (b) film state.

https://doi.org/10.1007/s10118-026-3853-9

sion peaks of PCFDF-DT-DN$_x$ with increasing DN content (x value). However, because of the very low DN content, the emission peak attributed to the DN units in PCFDF-DT-DN$_x$ was not clearly observable in solution.[24] However, in the solid thin-film state (Fig. 4b), all the polymers exhibited a single broad emission peak in the range of 425–670 nm. This phenomenon confirms that, under the tight molecular packing in the film, the excitation energy of the main chain can be completely captured and efficiently converted by the side-chain mCP and DN units.[33–35] More importantly, with an increase in the x value (*i.e.*, DN unit content), the emission peak of PCFDF-DT-DN$_x$ in the film state showed a significant red shift and intensity enhancement, and the peak shape gradually broadened, covering almost the entire visible-light region. This change is directly attributed to the film aggregation effect, which significantly promotes the electronic coupling between chromophores and improves the efficiency of Förster resonance energy transfer (FRET).[36] Additionally, the photoluminescence quantum yield (PLQY) of PCFDF-DT-DN$_x$ in oxygen-free neat films was measured to be 8.97%, 9.46%, 9.57%, 8.74%, 7.81%, 9.36%, and 7.31%, respectively. These spectral changes indicate that the intermolecular and intramolecular energy transfer processes have a significant impact on the photophysical properties of the polymers, laying an important photophysical foundation for the subsequent continuous regulation of the emission color and even white-light emission.

To further elucidate the intermolecular energy transfer mechanism and investigate the theoretical basis for color tuning and white light emission based on the red, green, and blue (RGB) three-primary-color system, we compared the PL spectrum of PCFDF-DT-DN$_0$ with the UV-Vis absorption spectrum of DN-Ikyne. PCFDF-DT-DN$_0$ contains the green TADF units (DT) in the main chain and the blue fluorescent units (mCP) attached to the side chain without any red-emitting component. As shown in Fig. 5, the UV-Vis absorption spectrum of DN-Alkyne exhibits distinct absorption peaks in the range of 380–562 nm, which partially overlap with the PL spectrum of PCFDF-DT-DN$_0$, satisfying the spectral overlap condition for FRET.[37–39] This mechanistic verification indicates that by further introducing the DN units into the polymer side chains in a controllable manner *via* click chemistry, the blue, green, and red primary-color emitting centers can be assembled within a single polymer molecule. This establishes a cascade energy transfer pathway from the polymer backbone, DT units, and mCP units to the DN units.[40] By precisely adjusting the molar ratios of the red-, green-, and blue-emitting units, the emission intensities of each channel can be balanced. This not only enables continuous tuning of the emission chromaticity over a wide range, but also achieves broad-spectrum white-light emission through cooperative color mixing of the three emissions. Thus, this work provides a solid theoretical and experimental foundation for the molecular design of SMWLEPs based on the three primary colors.[33,38]

To verify the delayed fluorescence characteristics of the polymers, the transient PL decay spectra of non-doped PCFDF-DT-DN$_x$ (x=0, 0.25, 0.5, 1.5, 2.5, 5, or 10) thin films were measured at 298 K under a nitrogen atmosphere, as depicted

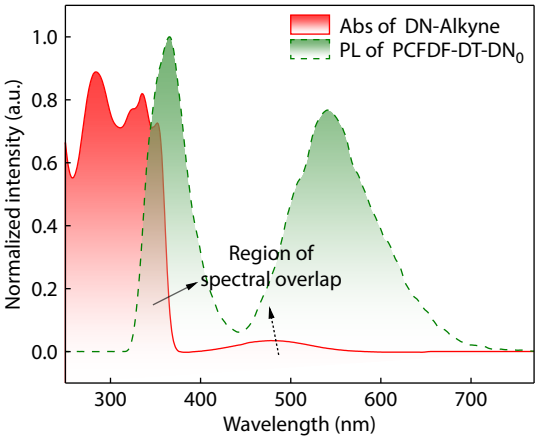


Fig. 5 PL spectra of PCFDF-DT-DN$_0$ and UV-Vis absorption spectrum of DN-Alkyne in chloroform solution.

in Fig. S27 (in ESI). All the polymers exhibited bi-exponential decay kinetics, with two distinct lifetime components in the film state. The prompt fluorescence lifetime ranges from 8.90 ns to 11.24 ns, whereas the delayed fluorescence lifetime is in the range of 1.16–2.37 μs. The detailed kinetic parameters are summarized in Table S3 (in ESI). These results confirm that the target polymers successfully inherited the intrinsic TADF characteristics of the small-molecule precursors.[30,41]

To investigate the electrochemical properties of the target polymers, CV measurements were performed on the PCFDF-DT-DN$_x$ film, and the results are shown in Fig. S28 (in ESI). With the increase in the value of x, the intensity of the oxidation characteristic peak attributed to DN unit at 0.99 eV gradually increases, while the peak attributed to mCP unit around 1.18 eV gradually decreases. Notably, the positions of the two oxidation peaks do not show obvious shifts regardless of the DN unit/mCP unit molar ratio, indicating that the target polymers successfully inherit the electrochemical properties of the side-chain units. Moreover, it can be inferred that connecting the two TADF emissive units through non-conjugated alkyl chains can greatly suppress their interactions, which is more conducive to the polymers inheriting the electrochemical properties of the side-chain small molecules.[40,42] The highest occupied molecular orbital (HOMO) energy level, lowest unoccupied molecular orbital (LUMO) energy level, and optical band gap of the polymers were calculated from the UV-Vis absorption spectra in solution and the onset potential of the oxidation peak in the CV curves. According to the formula $E_{LUMO} = E_{HOMO} + E_g$,[30,31] the HOMO energy levels of PCFDF-DT-DN$_x$ are distributed between –5.28 and –5.23 eV, and the LUMO energy levels are in the range of –2.30 to –2.25 eV. The detailed data related to the thermal, photophysical, and electrochemical properties of PCFDF-DT-DN$_x$ are summarized in Table 1.

Electroluminescence Performance

To systematically evaluate the electroluminescence (EL) properties of the PCFDF-DT-DN$_x$, the non-doped OLED devices were fabricated by spin-coating PCFDF-DT-DN$_x$ (x=0, 0.25, 0.5, 1.5, 2.5, 5, or 10) as the emissive layer (EML), and the corresponding non-doped devices were named as ND-0, ND-0.25, ND-0.5, ND-1.5, ND-2.5, ND-5, and ND-10, respectively. The device structure and

energy-level diagram are shown in Fig. S29 (in ESI). The EL spectra of the devices, CIE coordinates at maximum luminance, EL spectra of device ND-10 at 3–9 V, current efficiency-current density curves, current density-voltage-luminance (*J-V-L*) curves, and external quantum efficiency (EQE)-current density curves are shown in Fig. 6. Detailed EL performance data all devices are summarized in Table 2.

As shown in Fig. 6(a), at the maximum luminance, the EL spectra of ND-0–ND-10 show an emission peak in the range of 425–835 nm, indicating excellent color tunability and broad-spectrum emission potential. Except for ND-10, the devices with lower DN content exhibited only a green emission peak that continuously red-shifted from 522 nm to 530 nm, while no red emission peak appeared. The spectral shape is

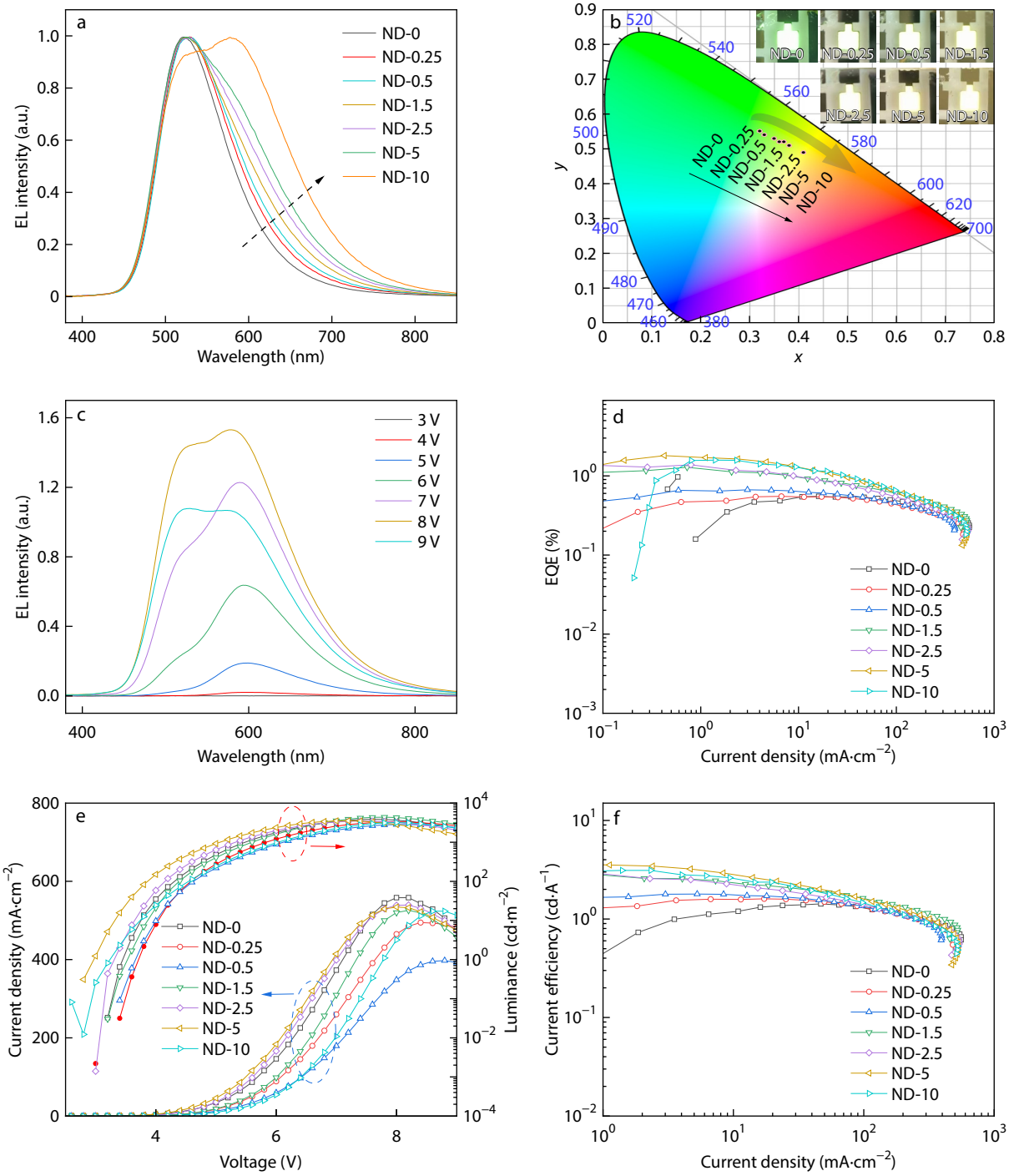


Fig. 6 (a) Normalized EL spectra of device ND-0–ND-10; (b) The CIE coordinates at maximum brightness of ND-0–ND-10; (c) EL spectra of device ND-10 at operating voltages of 3–9 V; (d) Current efficiency-current density curves of device ND-0–ND-10; (e) Current density-voltage-luminance curves of device ND-0–ND-10; (f) EQE-current density curves of device ND-0–ND-10.

https://doi.org/10.1007/s10118-026-3853-9

similar to that of the PL emission peaks of the polymer films. Although the EL spectra are generally similar in shape to the PL spectra, some differences still exist. Specifically, the weak shoulder peak at 416 nm, which is assigned to the intrinsic emission of the carbazole-fluorene backbone, is present in the PL spectra but completely disappears in the EL spectra. This difference is primarily attributable to the distinct excitation mechanisms involved. In the PL process, uniform photon excitation allows the polymer backbone to be independently excited; however, incomplete energy transfer results in the persistence of a shoulder peak originating from the backbone itself. In contrast, in the EL process, excitation relies on charge injection and subsequent recombination. The charge carriers are preferentially captured by the TADF units, leaving the backbone nearly incapable of forming effective excitons. As a consequence, the emission peak at 416 nm vanishes.[43,44] Notably, as the DN content increased, the emission peak gradually red-shifted and broadened. These changes indicate an enhanced and complete energy transfer efficiency from the polymer backbone, DT units, and mCP units to the DN units. However, ND-10 shows two emission peaks at 522 and 579 nm, which are assigned to mCP units, DT units, Cz-Br/F-BO-based segments and the DN units, respectively. Their superposition covers almost the entire visible region, indicating incomplete energy transfer from green TADF units and blue fluorescence units to red TADF units. In addition, the EL peak intensity at 522 nm clearly decreased, whereas a distinct EL peak appeared at 579 nm. This phenomenon suggests that by controlling the molar ratios of the three emitting units (DN, DT, and mCP, corresponding to red, green, and blue, respectively) to maintain incomplete energy transfer, the emission intensities of red, green, and blue can be synergistically tuned. As a result (Fig. 6b and Table 2), the CIE coordinates shifted gradually from (0.32, 0.55) to (0.41, 0.49), and the correlated color temperature (CCT) decreased from 5763 K to 3920 K. This reflects a continuous color evolution from cold green to yellowish green, and then to near-warm white, which is fully consistent with the movement trajectory of the points in the CIE chromaticity diagram.

These results indicate that by fixing the DT content in the main chain and simply adjusting the content of DN units introduced into the side chains, broad-range color tuning and even near-warm white emission can be achieved in a single-molecule polymer. However, standard white-light emission has not been directly achieved. To investigate the reason, we compared our work with the recent work of Wu *et al*.[25] In their work, they attached the same red- and green-emitting units (DN and DT units) to the side chains and successfully achieved white-light emission by adjusting their molar ratio. Combined with the structural features of PCFDF-DT-DN$_x$ (Scheme 1) and the EL spectral (Fig. 6a) analysis in this work, the main reasons for this are speculated as follows. After being embedded into the conjugated main chain, the green DT units form a strong conjugated extension effect. Although a blue fluorescent component (mCP) was introduced into the side chains, it failed to effectively suppress the red shift of the green emission peak. As a result, PCFDF-DT-DN$_0$ exhibited green emission rather than the expected blue-green emission. After further introducing the red DN units, the energy transfer preferentially proceeds toward the red channel, shifting the overall spectral center toward longer wavelengths. Consequently, the emission intensities of the three primary colors (red, green, and blue) deviated from the ideal white-light balance. Therefore, synergistic optimization of the emission intensities of the three primary colors in the current system has not yet been achieved. Further optimization of the main-chain conjugation length or the type and content of the blue component is required to achieve a standard white-light emission.

Furthermore, to evaluate the spectral and color stabilities, we measured the EL spectra and CIE coordinates of devices ND-0 to ND-10 under varying voltages (Fig. 6c; Figs. S30 and S31 in ESI). For ND-10, the EL spectra (425–835 nm) remained nearly unchanged at 3–8 V, but broadened significantly at 9 V owing to carrier imbalance and thermal effects. Notably, the green emission at 522 nm (from mCP units, DT units and Cz-Br/F-BO-based segments) increased with voltage. Accordingly, the CIE coordinates shifted from (0.48, 0.48) at 4 V to (0.41, 0.49) at 9 V, indicating an orange-to-warm-white transition (ΔCIE_x=0.07, ΔCIE_y=0.01). This voltage-dependent color shift arises from the different charge recombination dynamics among the green TADF, blue fluorescent, and red TADF units. At low voltages, blue-green-to-red energy transfer dominates, and the red units act as exciton traps, favoring hole injection into the DN units and yielding orange emission. At higher voltages, increased electron flow and a broader recombination zone enhanced the green emission, shifting the CIE coordinates toward warm white. These results agree well with the EL spectral changes, revealing notable color variations with voltage. To better understand the underlying origins of this voltage-dependent color shift and to guide future optimization, we further analyze the possible contributing factors below. This phenomenon is considered to originate from four main factors. First, the injection and transport bal-

Table 2 EL performances of the non-doped OLED devices ND-0–ND-10.

Devices	V_{on} [a] (V)	λ_{EL} [b] (nm)	L_{max} [c] (cd·m^{-2})	CE_{max} [d] (cd·A^{-1})	EQE_{max} [e] (%)	CIE [f] (x, y)	CCT [g] (K)	CRI [h]
ND-0	3.2	522	3866.7	1.42	0.45	(0.32, 0.55)	5763.3	79.0
ND-0.25	3.6	524	3329.7	1.60	0.55	(0.33, 0.54)	5396.7	81.0
ND-0.5	3.6	525	2833.5	1.79	0.67	(0.35, 0.53)	5211.5	81.9
ND-1.5	3.5	527	4365.6	2.89	1.28	(0.36, 0.52)	5050.6	88.9
ND-2.5	3.3	529	3466.2	2.95	1.37	(0.37, 0.52)	4828.9	84.2
ND-5	3.0	530	3532.0	3.68	1.81	(0.38, 0.51)	4647.9	85.3
ND-10	3.3	522, 579	3169.2	3.11	1.58	(0.41, 0.49)	3920.8	88.9

[a] Turn-on voltage at a luminance of 1 cd·m^{-2}; [b] EL emission peak; [c] Maximum luminance; [d] Maximum current efficiency; [e] Maximum external quantum efficiency; [f] CIE coordinates at maximum luminance; [g] Color temperature at maximum luminance; [h] Color rendering index at maximum luminance.

https://doi.org/10.1007/s10118-026-3853-9

ance of holes and electrons vary with applied voltage, causing the recombination zone to migrate within the emissive layer and thus altering the relative excitation weights of different emitting components.[45] Second, the enhanced electric field may influence exciton dissociation and energy transfer processes, leading to differential suppression especially of the short-wavelength components.[46] Third, Joule heating at higher voltages can induce subtle changes in molecular conformation and film morphology, which in turn perturb the spectral output.[47,48] Fourth, the distinct carrier capture cross-sections of each unit result in nonlinear responses to voltage, ultimately shifting the spectral composition.[48] To address these issues, several mitigation strategies are proposed, including optimizing the host material and doping ratio to balance carrier transport, introducing hole/electron blocking layers to confine the recombination zone within the center of the emissive layer, and performing molecular modification on the conjugated backbone to reduce the voltage sensitivity of each component.

Figs. 6(d) and 6(f) show the current efficiency-current density curves and external quantum efficiency (EQE)-current density curves of ND-0–ND-10, respectively. The evolution of EQE with the current density (J) showed three characteristic regions. In the low-current-density region (J<1 mA·cm^{-2}), the EQE increased rapidly with increasing J, owing to a gradual improvement in the charge carrier balance. In the plateau region (1<J<100 mA·cm^{-2}), the EQE reached its maximum value and remained relatively stable, signifying a highly efficient charge recombination. Finally, in the high-current density region (J>100 mA·cm^{-2}), the EQE decreased, primarily owing to exciton quenching mechanisms such as triplet-triplet annihilation (TTA) and Joule heating effects.[47] The J-V-L characteristics thus provide a comprehensive means to evaluate charge injection, transport, recombination efficiency, and operational stability of the OLEDs. Notably, for PCFDF-DT-DN$_x$ (x=0, 0.25, 0.5, 1.5, 2.5, 5, or 10), increasing the molar ratio of DN to DT from 0/50 to 5/50 and 10/50 shifted the J-V curves of the corresponding devices toward lower voltages, indicating enhanced charge injection and transport. This performance improvement is attributed to the synergistic effect of the conjugated main chain (enhancing hole transport) and the DN units (improving electron transport), which together optimize the exciton balance and promote efficient energy transfer in the emissive layer.[49] As shown in Table 2, both CE$_{max}$ and EQE$_{max}$ of ND-x (x=0, 0.25, 0.5, 1.5, 2.5, 5, or 10) gradually increased as the molar ratio of DN units to DT units of the PCFDF-DT-DN$_x$ EML changes from 0/50 to 10/50. Among the devices, ND-0 to ND-10, ND-5 exhibited the highest CE$_{max}$ and EQE$_{max}$. However, further increasing the DT/DN ratio to 10/50 led to slight decreases in CE$_{max}$ and EQE$_{max}$ for device ND-10. This suggests that an excessive DN content induces ACQ, resulting in reduced device efficiency.[50,51] If the DN content continues to increase, it is expected that both EQE and luminance will decrease further, and the CIE coordinates will also shift significantly away from the white-light region. This phenomenon is mainly attributed to the role of the DN unit as a narrow-bandgap red emitter, which acts as an exciton trap in the system. Excessively high DN content exacerbates non-radiative loss processes such as concentration quenching, TTA, and charge capture imbalance, ultimately compromising the device efficiency and spectral stability.[47,49,52–54] Therefore, future design of SMWLEPs should not only choose efficient long-wavelength emitters but also optimize their loading to boost the overall EL performance of WOLEDs.

Fig. 6(e) shows the current density-voltage-luminance (J-V-L) curves of ND-0–ND-10. Combined with the performance data in Table 2, it can be seen that all the OLED devices based on PCFDF-DT-DN$_x$ have a V_{on} lower than 3.6 V. This indicates that the energy levels of each functional layer of the device are well matched, with low charge injection barriers. Meanwhile, the L_{max} of the device series ranges from 2833.5 cd·m^{-2} to 4365.6 cd·m^{-2}, demonstrating good luminous performance. This preliminarily confirms the good charge transport ability of the conjugated polymer backbone and the significant advantage of TADF luminescent materials in improving the exciton utilization efficiency. In terms of the overall device performance, ND-5 exhibited the best performance among the non-doped devices. It has a V_{on} of 3.0 V, a L_{max} of 3532.0 cd·m^{-2}, a CE$_{max}$ of 3.68 cd·A^{-1}, and an EQE$_{max}$ of 1.81%. Notably, the ND-10 device achieved warm white light emission with the CIE coordinates of (0.41, 0.49), a CCT of 3920 K, and a CRI of 88.9. Furthermore, it has a V_{on} of 3.3 V, a L_{max} of 3169.2 cd·m^{-2}, and an EQE$_{max}$ of 1.58%. It shows good application potential in solution-processed WOLEDs.

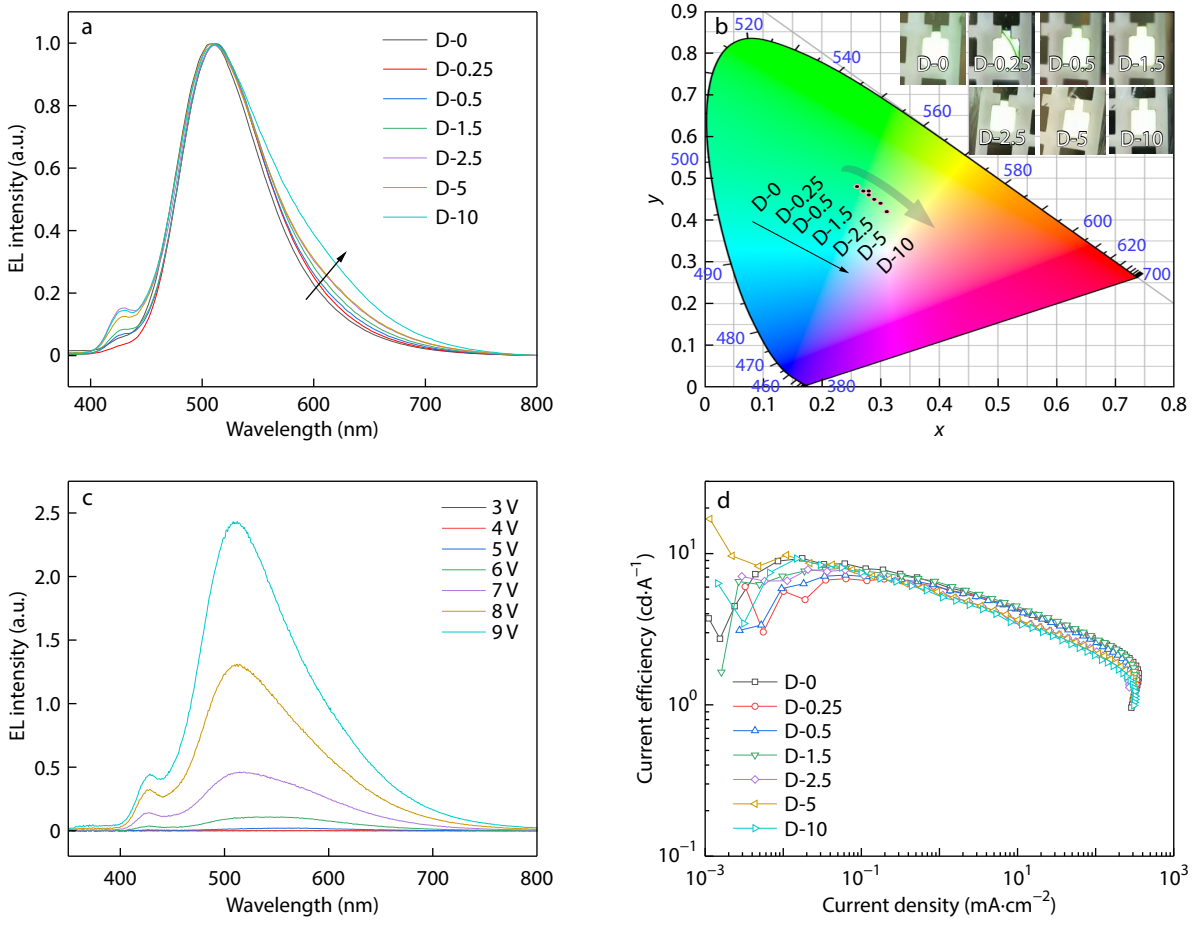
Furthermore, our devices were compared with previously reported non-doped devices based on SMWLEPs, and the relevant data are summarized in Table S4 (in ESI). Compared with the reported devices, the ND-5 and ND-10 devices in this work exhibited better CRI. Their V_{on}, L_{max}, CE$_{max}$, and EQE$_{max}$ were significantly higher than those of PFSOTT0.05, PFSOTT0.1, and PDFC-DT$_{97}$-TB$_3$.[24,55,56] This indicates that the conjugated main chain facilitates efficient hole transport and suppresses charge accumulation. However, Wu *et al*.[25] attached the same red and green units (DN and DT) to the side chains and successfully achieved white-light emission with higher CE$_{max}$ and EQE$_{max}$. It is suggested by a comparative analysis that, in our work, embedding the DT units into the conjugated main chain causes a red-shift of the green emission owing to the conjugated extension effect, and the blue fluorescent mCP units cannot fully balance the emission, resulting in near-warm white light. Meanwhile, the energy transfer efficiency is weakened by the increased spatial distance between the DT and DN units, and extra energy dissipation is added by the introduction of the blue component, leading to relatively lower CE$_{max}$ and EQE$_{max}$. To better understand why our current backbone design leads to lower EQE, we compared our polymer structure with that of Wu *et al*. The main difference is that Wu *et al*.'s polymer contains only carbazole and fluorene units, whereas our polymer incorporates an additional green TADF unit (based on triazine acridine) along with the carbazole and fluorene backbone. This structural difference affects device performance in several ways. First, the donor-acceptor nature of the triazine-acridine unit creates ICT states. These states may couple with the delocalized excited states of the backbone. As a result, extra non-radiative decay paths are introduced.[57] Second, the bulky triazine-acridine group increases molecular disorder. Moreover, the deep LUMO level of triazine tends to form trap sites. These trap sites can quench excitons.[29,58] Third, our polymers have PLQY values of only 7.31%–9.57%. This is much

lower than that of Wu *et al.*'s material.[25] The low PLQY directly limits the upper bound of EQE. Fourth, the imbalance of carrier injection and transport is also critical.[52] Perhaps our backbone design does not achieve optimal matching between holes and electrons. Thus, some carriers are lost before recombination. The observed CIE coordinate shift with voltage also confirms the migration of the recombination zone and the lack of carrier balance. These factors further reduce EQE. In summary, while the TADF unit is capable of harvesting triplet excitons, its incorporation also gives rise to multiple exciton loss channels. Consequently, the EQE of our device is lower than that of the simpler carbazole fluorene backbone. These findings offer valuable guidance for the future design and optimization of conjugated polymers incorporating TADF units.

To further evaluate their EL properties, the doped OLED devices were fabricated using PCFDF-DT-DN$_x$ (x=0, 0.25, 0.5, 1.5, 2.5, 5 or 10) (10 wt%) in CBP as EML, respectively, and named as D-0, D-0.25, D-0.5, D-1.5, D-2.5, D-5, and D-10. Their EL performances are shown in Fig. 7 and summarized in Table 3.

Compared with the non-doped devices, the EL performance of the doped devices was significantly enhanced. Compared with ND-0, the performance of D-0 exhibits the most significant variation, the CE_{max} increases from 1.42 cd·A^{-1} to 9.29 cd·A^{-1}, the L_{max} increases from 3866.7 cd·m^{-2} to 5973.6 cd·m^{-2}, and the EQE_{max} increases from 0.45% to 4.79%. Among the D-0.25–D-10 devices, D-1.5 exhibited the best performance, with a CE_{max} of 8.00 cd·A^{-1}, a L_{max} of 5435.1 cd·m^{-2}, and an EQE_{max} of 5.84%. These results indicate that using CBP as the host material can enhance the charge transport capacity in the emissive layer, inhibit the intermolecular interactions in the thin film, and reduce the ACQ effect.[19,50,59] The V_{on} of the doped devices was slightly increased, which may be attributed to the increased hole injection barrier caused by the introduction of CBP. As shown in Fig. 7(a), compared with the non-doped devices, the EL spectra of the doped devices covered the entire visible range (400–800 nm). The peaks were slightly broadened and exhibited a minor blue shift. In addition, a weak emission peak appears at approximately 430 nm. This is presumably because the introduction of CBP leads to incomplete absorption of the emission from the main chain (green) or CBP itself (blue) to the red TADF units. In addition, as the DN content in PCFDF-DT-DN$_x$ (x=0, 0.25, 0.5, 1.5, 2.5, 5, or 10) increased, the EL spectra of the doped devices gradually broadened, and the CIE coordinates shifted from the initial green light region (0.27, 0.47) of D-0.25 to the cool white light region (0.31, 0.42) of D-10, indicating that the emission color shifted from green to cool white. Among them, the D-10 device has the emission color closest to cool white light, but it still deviates from the standard white light coordinate (0.33, 0.33), indicating that its white light purity requires further optimization.

To further evaluate the color stability of the doped devices, we compared the voltage-dependent CIE coordinates of ND-



https://doi.org/10.1007/s10118-026-3853-9

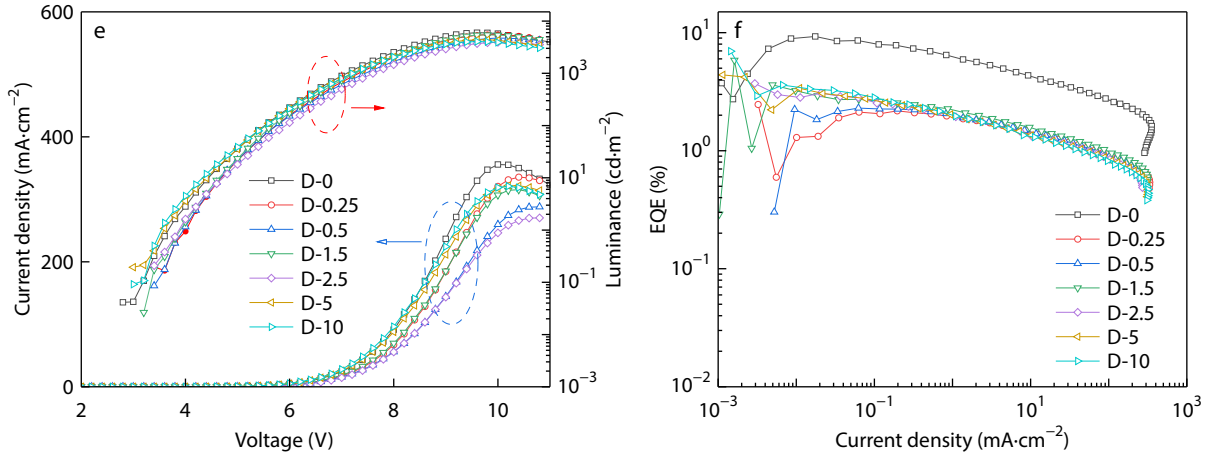


Fig. 7 (a) Normalized EL spectra of device D-0–D-10; (b) The CIE coordinates at the maximum brightness of D-0–D-10; (c) EL spectra of device D-10 at operating voltages of 3–9V; (d) Current efficiency-current density curves of device D-0–D-10; (e) Current density-voltage-luminance curves of device D-0–D-10; (f) EQE-current density curves of device D-0–D-10.

Table 3 EL performance of devices D-0–D-10 doped with CBP.

Devices	V_{on} [a] (V)	λ_{EL} [b] (nm)	L_{max} [c] (cd·m^{-2})	CE_{max} [d] (cd·A^{-1})	EQE_{max} [e] (%)	PLQY [f] (%)	CIE [g] (x, y)	CCT [h] (K)	CRI [i]
D-0	3.7	506	5973.6	9.29	4.79	17.73	(0.26, 0.48)	7400.6	76.9
D-0.25	4.0	507	5522.2	6.82	2.46	10.15	(0.27, 0.47)	6900.8	77.2
D-0.5	4.0	509	4730.6	7.20	2.30	13.30	(0.28, 0.47)	6905.0	78.9
D-1.5	4.0	511	5435.1	8.00	5.84	10.89	(0.28, 0.46)	6780.4	80.1
D-2.5	3.9	512	4018.4	7.79	3.71	13.28	(0.29, 0.45)	6882.3	82.6
D-5	3.6	515	4378.8	16.93	4.38	12.46	(0.30, 0.46)	6882.1	81.8
D-10	3.6	517	4050.9	9.26	3.96	7.76	(0.31, 0.42)	6386.0	84.7

[a] Turn-on voltage at a luminance of 1 cd·m^{-2}; [b] EL emission peak; [c] Maximum luminance; [d] Maximum current efficiency; [e] Maximum external quantum efficiency; [f] Photoluminescence quantum yield in the thin-film state; [g] CIE coordinates at maximum luminance; [h] Color temperature at maximum luminance; [i] Color rendering index at maximum luminance.

10 and D-10. As shown in Fig. S32 (in ESI), the coordinates of ND-10 shift from (0.48, 0.48) at 4 V to (0.41, 0.49) at 9 V, showing a significant change (Δ_x=0.07, Δ_y=0.01). In contrast, D-10 only changes slightly from (0.33, 0.40) to (0.31, 0.42), with much smaller offsets (Δ_x=0.02, Δ_y=0.02). This indicates that the incorporation of the CBP host significantly improves the color stability. This improvement can be attributed to the ability of CBP, as a wide-bandgap host, to balance carrier transport and suppress the migration of the recombination zone, thereby stabilizing the emission intensities of different components.[59] Therefore, the proper selection of the host material is of great importance for enhancing the spectral stability and color reliability of white OLEDs.

Although the non-doped devices based on the "main-chain/side-chain synergy" strategy have achieved low turn-on voltage, high luminance, and near-warm white emission, there is still room for improvement. First, the CIE coordinates deviate from the standard white point (0.33, 0.33). This deviation is attributed to the intrinsic redshift caused by incorporating green-emitting units into the main chain, or to the mismatched energy levels among the three primary-color units and the non-optimal feed ratio for white balance. Second, the overall electroluminescence efficiency is lower than that of high-efficiency TADF copolymers, doped systems, and host-guest systems. Studies have shown that small-molecule or sensitized systems can achieve an EQE_{max} of more than 10% or even 20%,[4,33,60] whereas our single-component polymers suffer from aggregation and exciton quenching, resulting in relatively low efficiency. In addition, carrier imbalance under operating conditions aggravates non-radiative recombination, further limiting the EQE improvement.[19,61]

To promote the efficient and stable development of non-doped WOLEDs, the future optimization directions are as follows: first, we will develop new TADF emitters (either three-primary-color or complementary-color) with matched energy levels to improve white-light purity and radiative recombination. Second, we will precisely tune the molar ratios of the emitting units to determine the optimal loading of red-emitting units, thereby achieving efficient exciton utilization and standard white emission. Third, we will introduce a host material with high carrier mobility and high exciton utilization to optimize the energy-level alignment and charge-transport balance, thus suppressing quenching. Our group will further extend the conjugated main-chain structures and design new single-component TADF white-light polymers with novel topologies. We will also explore the structure-property-device performance relationships, aiming to advance the application of solution-processed WOLEDs in lighting and displays.

CONCLUSIONS

In summary, a series of conjugated polymers, PCFDF-DT-DN_x (x=0, 0.25, 0.5, 1.5, 2.5, 5, or 10), with a synergistic main-chain/side-chain design was successfully synthesized. The con-

jugated main chain containing green TADF units was synthesized *via* Suzuki polymerization, and the red TADF units were attached to the side chain *via* a post-click reaction. This synthetic strategy addresses the drawbacks of traditional copolymer systems, such as poorly controlled composition, complicated synthesis, and low reproducibility. Moreover, the main-chain/side-chain synergistic effect enables PCFDF-DT-DN$_x$ to exhibit good charge-transporting ability and facile emission color tunability. Notably, the non-doped device based on PCFDF-DT-DN$_{10}$ achieves warm white emission with CIE coordinates of (0.41, 0.49), a L_{max} of 3169.2 cd·m^{-2}, a V_{on} of 3.3 V, and an EQE$_{max}$ of 1.58%. The CBP-doped device D-10 realized efficient cold white emission, with EQE$_{max}$ and L_{max} increasing to 3.96% and 4050.9 cd·m^{-2}, respectively. This work provides a new molecular design concept for SMWLEPs, potentially advancing their practical use in high-performance solution-processable WOLEDs.

Conflict of Interests

The authors declare no interest conflict.

Electronic Supplementary Information

Electronic supplementary information (ESI) is available free of charge in the online version of this article at http://doi.org/10.1007/s10118-026-3853-9.

Data Availability Statement

The data supporting the findings of this study are available from the corresponding author upon reasonable request.

ACKNOWLEDGMENTS

This work was financially supported by the National Natural Science Foundation of China (No. U2004173), the Key Scientific Research Project of Colleges and Universities in Henan Province (No. 24A430043), and the Open Fund of the State Key Laboratory of Luminescent Materials and Devices (South China University of Technology) (No. 2020-skilled-08).

REFERENCES

1 Barah, D.; Ray, D. Broadband white electroluminescence from a dopant-free OLED comprising pure electromer and electroplex emission. *J. Phys. D: Appl. Phys.* **2024**, *57*, 135312.
2 Liu, Y.; Zhu, F.; Wang, Y.; Yan, D. High-efficiency crystalline white organic light-emitting diodes. *Light Sci. Appl.* **2024**, *13*, 86.
3 Yang, N.; Yue, G.; Zhang, Y.; Qin, X.; Gao, Z.; Mi, B.; Fan, Q.; Qian, Y. Reproducible and high-performance WOLEDs based on independent high-efficiency triplet harvesting of yellow hot-exciton esipt and blue TADF emitters. *Small* **2024**, *20*, 2304615.
4 Ding, D.; Wang, Z.; Li, C.; Zhang, J.; Duan, C.; Wei, Y.; Xu, H. Highly efficient and color-stable thermally activated delayed fluorescence white light-emitting diodes featured with single-doped single emissive layers. *Adv. Mater.* **2020**, *32*, e1906950.
5 Chen, J. X.; Wang, K.; Xiao, Y. F.; Cao, C.; Tan, J. H.; Wang, H.; Fan, X. C.; Yu, J.; Geng, F. X.; Zhang, X. H.; Lee, C. S. Thermally activated delayed fluorescence warm white organic light emitting devices with external quantum efficiencies over 30%. *Adv. Funct. Mater.* **2021**, *31*, 2101647.
6 Dong, R.; Liu, D.; Li, J.; Ma, M.; Mei, Y.; Li, D.; Jiang, J. Acceptor modulation for blue and yellow TADF materials and fabrication of all-TADF white OLED. *Mater. Chem. Front.* **2021**, *6*, 40–51.
7 Zhang, T.; Xiao, Y.; Wang, H.; Kong, S.; Huang, R.; Ka-Man Au, V.; Yu, T.; Huang, W. Highly twisted thermally activated delayed fluorescence (TADF) molecules and their applications in organic light-emitting diodes (OLEDs). *Angew. Chem.* **2023**, *135*, e202301896.
8 Kothavale, S.; Kim, S. C.; Cheong, K.; Zeng, S.; Wang, Y.; Lee, J. Y. Solution-processed pure red TADF organic light-emitting diodes with high external quantum efficiency and saturated red emission color. *Adv. Mater.* **2023**, *35*, 2208602.
9 C P, K. P.; Naveen, K. R.; Hur, J. Acceptor–donor–acceptor based thermally activated delayed fluorescent materials: structure–property insights and electroluminescence performances. *Mater. Chem. Front.* **2024**, *8*, 769–784.
10 Zhu, Y.; Zhang, Y.; Yao, B.; Wang, Y.; Zhang, Z.; Zhan, H.; Zhang, B.; Xie, Z.; Wang, Y.; Cheng, Y. Synthesis and electroluminescence of a conjugated polymer with thermally activated delayed fluorescence. *Macromolecules* **2016**, *49*, 4373–4377.
11 da Silva Candido, L.; Barbosa de Brito, E.; Corrêa Santos, D.; de Fátima Vieira Marques, M. Advances in polymeric white light-emitting OLEDs for high-efficiency lighting applications. *J. Mater. Sci. Mater. Electron.* **2025**, *36*, 561.
12 Huang, M.; Chen, Z.; Miao, J.; He, S.; Yang, W.; Huang, Z.; Zou, Y.; Gong, S.; Tan, Y.; Yang, C. Harmonization of rapid triplet up-conversion and singlet radiation enables efficient and stable white OLEDs. *Nat. Commun.* **2024**, *15*, 8048.
13 Schwartz, G.; Pfeiffer, M.; Reineke, S.; Walzer, K.; Leo, K. Harvesting triplet excitons from fluorescent blue emitters in white organic light-emitting diodes. *Adv. Mater.* **2007**, *19*, 3672–3676.
14 Li, W.; Li, B.; Cai, X.; Gan, L.; Xu, Z.; Li, W.; Liu, K.; Chen, D.; Su, S. J. Tri-spiral donor for high efficiency and versatile blue thermally activated delayed fluorescence materials. *Angew. Chem. Int. Ed.* **2019**, *58*, 11301–11305.
15 Kim, G. W.; Bae, H. W.; Lampande, R.; Ko, I. J.; Park, J. H.; Lee, C. Y.; Kwon, J. H. Highly efficient single-stack hybrid cool white OLED utilizing blue thermally activated delayed fluorescent and yellow phosphorescent emitters. *Sci. Rep.* **2018**, *8*, 16263.
16 Zhang, J.; Han, C.; Du, F.; Duan, C.; Wei, Y.; Xu, H. High-power-efficiency white thermally activated delayed fluorescence diodes based on selectively optimized intermolecular interactions. *Adv. Funct. Mater.* **2020**, *30*, 2005165.
17 Huang, C.; Zhang, Y.; Zhou, J.; Sun, S.; Luo, W.; He, W.; Wang, J.; Shi, X.; Fung, M. K. Hybrid tandem white OLED with long lifetime and 150 Lm W^{-1} in luminous efficacy based on TADF blue emitter stabilized with phosphorescent red emitter. *Adv. Opt. Mater.* **2020**, *8*, 2000727.
18 Duan, C.; Li, Z.; Zhang, J.; Han, C.; Xu, H. Direct evidence of dopant-dopant synergism in efficient single-emissive-layer white thermally activated delayed fluorescence. *Nano Energy* **2021**, *89*, 106358.
19 Khammultri, P.; Chasing, P.; Chitpakdee, C.; Namuangruk, S.; Sudyoadsuk, T.; Promarak, V. Red to orange thermally activated delayed fluorescence polymers based on 2-(4-(diphenylamino)-phenyl)-9*H*-thioxanthen-9-one-10,10-dioxide for efficient solution-processed OLEDs. *RSC Adv.* **2021**, *11*, 24794–24806.
20 Fo, W. Z.; Li, J.; Zhang, Z. L.; Wei, B.; Zhang, Q. High-efficiency blue fluorescent OLEDs enabled by a cost-effective blade-coated

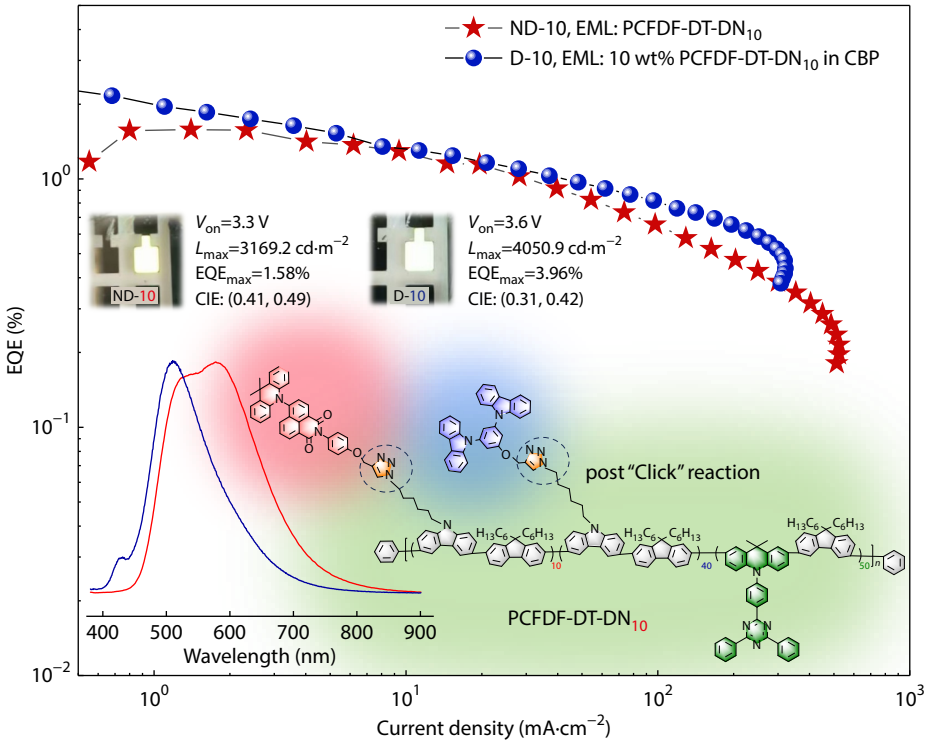
Graphical Abstract

Main-chain/Side-chain Synergistic Thermally Activated Delayed Fluorescence Conjugated Polymers for White Organic Light-emitting Diodes

Ming-Xiao Liu, Kai Jiang, Shao-Kui Cao, Zheng-Hao Zhao, Ming-Liang Zhao, Kun-Lun Wang, Ying-Liang Liu, Er-Gang Wang, Shi-Jian Su, and Shen-Gang Xu

Zhengzhou University, China; Huanghe Science & Technology University, China; South China University of Technology, China; Chalmers University of Technology, Sweden

Employing a synergistic main-chain/side-chain molecular design, a conjugated polymer light-emitting material with thermally activated delayed fluorescence (TADF) units incorporated in both the main chain and side chains was synthesized. The conjugated main chain facilitates charge transport, and the side chains provide versatile color adjustability. Ultimately, both doped and undoped devices exhibited near-white emission with high brightness and low turn-on voltage.



Chinese J. Polym. Sci. 2026 *https://doi.org/10.1007/s10118-026-3853-9*

planar source evaporation strategy. *Chem. Eng. J.* **2025**, *520*, 166364.

21 Tselekidou, D.; Papadopoulos, K.; Andrikopoulos, K. C.; Andreopoulou, A. K.; Kallitsis, J. K.; Logothetidis, S.; Laskarakis, A.; Gioti, M. Optical, photophysical, and electroemission characterization of blue emissive polymers as active layer for OLEDs. *Nanomaterials* **2024**, *14*, 1623.

22 Tselekidou, D.; Papadopoulos, K.; Foris, V.; Kyriazopoulos, V.; Andrikopoulos, K. C.; Andreopoulou, A. K.; Kallitsis, J. K.; Laskarakis, A.; Logothetidis, S.; Gioti, M. A comparative study between blended polymers and copolymers as emitting layers for single-layer white organic light-emitting diodes. *Materials* **2024**, *17*, 76.

23 Wang, T.; Song, X.; Huang, Z.; Miao, J.; Chen, Z.; Cheng, Y.; Yang, C. Color-tunable TADF conjugated polymers toward voltage-regulating white OLEDs for intelligent lighting. *Adv. Opt. Mater.* **2024**, *12*, 2303067.

24 Li, W.; Liu, D.; Ma, C.; Tao, Z.; Zhao, M.; Wang, K.; Liu, Y.; Cao, S.; Su, S. J.; Xu, S. Nonconjugated polymer flexibly linked with blue and orange-red thermally activated delayed fluorescence (TADF) units for white organic light-emitting diodes (WOLEDs). *ACS Appl. Polym. Mater.* **2025**, *7*, 12978–12988.

25 Wu, Y.; Liu, D.; Yang, L.; Yin, X.; Wang, K.; Liu, Y.; Wang, E.; Cao, S.; Su, S. J.; Xu, S. Precise synthesis of conjugated polymers grafted with red/green TADF units *via* postfunctionalization for single-molecule white electroluminescence. *Macromolecules* **2026**, *59*,

3541−3550.
26 Cao, Q.; Zhang, W.; Xu, H.; Wang, J.; Pei, M.; Qian, Y.; Zhou, T.; Zhang, K.; Ban, X. Efficient TADF polymer with optimized molecular structure and interaction for constructing solution-processed hybrid white OLEDs with EQE above 26%. *Chem. Eng. J.* **2023**, *466*, 143088.
27 Liu, D.; Wang, F.; Yao, R. Molecular evolution of host materials by regular tuning of N/p ratio for high-performance phosphorescent organic light-emitting diodes. *J. Mater. Chem. C* **2018**, *6*, 7839−7846.
28 Wang, B.; Zheng, Y.; Wang, T.; Ma, D.; Wang, Q. 1,8-Naphthalimide-based hybrids for efficient red thermally activated delayed fluorescence organic light-emitting diodes. *Org. Electron*. **2021**, *88*, 106012.
29 Lu, Y.; Liu, D.; Zhao, J.; Yin, X.; Wang, K.; Liu, Y.; Xu, S.; Su, S. J.; Cao, S. Solution-processable orange-red thermally activated delayed fluorescence hyper-structured molecular emitters containing diphenylamine substituted carbazole host units. *Dyes Pigm.* **2023**, *219*, 111548.
30 Zong, W.; Qiu, W.; Yuan, P.; Wang, F.; Liu, Y.; Xu, S.; Su, S. J.; Cao, S. Thermally activated delayed fluorescence polymers for high-efficiency solution-processed non-doped OLEDs: convenient synthesis by binding TADF units and host units to the pre-synthesized polycarbazole-based backbone *via* click reaction. *Polymer* **2022**, *240*, 124468.
31 Wang, F.; Qiu, W.; Zeng, J.; Yuan, P.; Zong, W.; Wu, W.; Liu, Y.; Xu, S.; Su, S. J.; Cao, S. Calix[4]resorcinarene-based hyper-structured molecular thermally activated delayed fluorescence yellow-green emitters for non-doped OLEDs. *J. Mater. Chem. C* **2020**, *8*, 4469−4476.
32 Sun, Y.; Xu, Z.; Wang, Y.; Niu, Z.; Xu, Z.; Li, S.; Wang, W.; Liu, Y. Enhanced performance of thermally activated delayed fluorescent light emitting diodes by optimized host polarity. *Opt. Express* **2024**, *32*, 17942.
33 Li, C.; Xu, Y.; Liu, Y.; Ren, Z.; Ma, Y.; Yan, S. Highly efficient white-emitting thermally activated delayed fluorescence polymers: synthesis, non-doped white OLEDs and electroluminescent mechanism. *Nano Energy* **2019**, *65*, 104057.
34 Li, C.; Ren, Z.; Sun, X.; Li, H.; Yan, S. Deep-blue thermally activated delayed fluorescence polymers for nondoped solution-processed organic light-emitting diodes. *Macromolecules* **2019**, *52*, 2296−2303.
35 Hu, Y.; Cai, W.; Ying, L.; Chen, D.; Yang, X.; Jiang, X. F.; Su, S.; Huang, F.; Cao, Y. Novel efficient blue and bluish-green light-emitting polymers with delayed fluorescence. *J. Mater. Chem. C* **2018**, *6*, 2690−2695.
36 Bertran, A.; Morbiato, L.; Sawyer, J.; Dalla Torre, C.; Heyes, D. J.; Hay, S.; Timmel, C. R.; Di Valentin, M.; De Zotti, M.; Bowen, A. M. Direct comparison between Förster resonance energy transfer and light-induced triplet-triplet electron resonance spectroscopy. *J. Am. Chem. Soc.* **2023**, *145*, 22859−22865.
37 Ye, S.; Bao, Y. Recent advances in fluorescent polymers with color-tunable aggregate emission. *Chem. Mater.* **2024**, *36*, 5878−5896.
38 Kyu Lee, S.; Jung, B. J.; Ahn, T.; Kwan Jung, Y.; Lee, J. I.; Kang, I. N.; Lee, J.; Park, J. H.; Ku Shim, H. White electroluminescence from a single polyfluorene containing bis-DCM units. *J. Polym. Sci. A Polym. Chem.* **2007**, *45*, 3380−3390.
39 Qi, Z.; Xie, J.; Chen, Q.; Gong, S.; Xie, G. Color-stable and highly efficient solution-processed white OLEDs with a copper(i) complex as a sensitizer. *J. Mater. Chem. C* **2025**, *13*, 9339−9346.
40 Yang, Y.; Zhao, L.; Wang, S.; Ding, J.; Wang, L. Red-emitting thermally activated delayed fluorescence polymers with poly(fluorene-*co*-3,3′-dimethyl diphenyl ether) as the backbone. *Macromolecules* **2018**, *51*, 9933−9942.
41 Kosai, J.; Masuda, Y.; Chikayasu, Y.; Takahashi, Y.; Sasabe, H.; Chiba, T.; Kido, J.; Mori, H. *S*-vinyl sulfide-derived pendant-type sulfone/phenoxazine-based polymers exhibiting thermally activated delayed fluorescence: synthesis and photophysical property characterization. *ACS Appl. Polym. Mater*. **2020**, *2*, 3310−3318.
42 Kim, M.; Jeon, S. K.; Hwang, S. H.; Lee, J. Y. Stable blue thermally activated delayed fluorescent organic light-emitting diodes with three times longer lifetime than phosphorescent organic light-emitting diodes. *Adv. Mater.* **2016**, *28*, 603.
43 Palmeira, T.; Berberan-Santos, M. N. Kinetic criteria for optimal thermally activated delayed fluorescence in photoluminescence and in electroluminescence. *J. Phys. Chem. C* **2017**, *121*, 701−708.
44 Gan, L.; Li, X.; Cai, X.; Liu, K.; Li, W.; Su, S. J. D-A-D-type orange-light emitting thermally activated delayed fluorescence (TADF) materials based on a fluorenone unit: simulation, photoluminescence and electroluminescence studies. *Beilstein J. Org. Chem.* **2018**, *14*, 672−681.
45 Bai, J.; Liu, X.; Chi, X.; Tang, A.; Zhang, H.; Ji, W. Diagnosing the charge dynamic behaviors in quantum-dot light-emitting diodes by temperature-dependent measurements. *J. Phys. Chem. Lett.* **2024**, *15*, 11847−11854.
46 Hariharan, M.; Kamat, P. Tuning excited-state energy transfer for light energy conversion: a virtual issue. *ACS Energy Lett.* **2022**, *7*, 2114−2117.
47 Nakanotani, H.; Higuchi, T.; Furukawa, T.; Masui, K.; Morimoto, K.; Numata, M.; Tanaka, H.; Sagara, Y.; Yasuda, T.; Adachi, C. High-efficiency organic light-emitting diodes with fluorescent emitters. *Nat. Commun.* **2014**, *5*, 4016.
48 Molina-Valdovinos, S.; Gurevich, Y. G. Nonlinear charge transport in bipolar semiconductors due to electron heating. *Phys. Lett. A* **2016**, *380*, 2021−2024.
49 Yang, Y.; Yang, L.; Li, X.; Zhao, L.; Wang, S.; Ding, J.; Wang, L. Trap-controlled white electroluminescence from a single red-emitting thermally activated delayed fluorescence polymer. *Front. Chem.* **2020**, *8*, 287.
50 Wang, T.; Li, K.; Yao, B.; Chen, Y.; Zhan, H.; Xie, Z.; Xie, G.; Yi, X.; Cheng, Y. Rigidity and polymerization amplified red thermally activated delayed fluorescence polymers for constructing red and single-emissive-layer white OLEDs. *Adv. Funct. Mater.* **2020**, *30*, 2002493.
51 Liu, J.; Xie, Z. Y.; Cheng, Y. X.; Geng, Y. H.; Wang, L. X.; Jing, X. B.; Wang, F. S. Molecular design on highly efficient white electroluminescence from a single-polymer system with simultaneous blue, green, and red emission. *Adv. Mater.* **2007**, *19*, 531−535.
52 Zhao, Z.; Liu, Y.; Hua, L.; Yan, S.; Ren, Z. Activating energy transfer tunnels by tuning local electronegativity of conjugated polymeric backbone for high-efficiency OLEDs with low efficiency roll-off. *Adv. Funct. Mater.* **2022**, *32*, 2200018.
53 Li, C.; Duan, L.; Sun, Y.; Li, H.; Qiu, Y. Charge transport in mixed organic disorder semiconductors: trapping, scattering, and effective energetic disorder. *J. Phys. Chem. C* **2012**, *116*, 19748−19754.
54 Serdiuk, I. E.; Ryoo, C. H.; Kozakiewicz, K.; Mońka, M.; Liberek, B.; Park, S. Y. Twisted acceptors in the design of deep-blue TADF emitters: crucial role of excited-state relaxation in the photophysics of methyl-substituted *s*-triphenyltriazine derivatives. *J. Mater. Chem. C* **2020**, *8*, 6052−6062.
55 Wang, Y.; Zhu, Y.; Xie, G.; Zhan, H.; Yang, C.; Cheng, Y. Bright white electroluminescence from a single polymer containing a

thermally activated delayed fluorescence unit and a solution-processed orange OLED approaching 20% external quantum efficiency. *J. Mater. Chem. C* **2017**, *5*, 10715−10720.
56 Khammultri, P.; Kitisriworaphan, W.; Chasing, P.; Namuangruk, S.; Sudyoadsuk, T.; Promarak, V. Efficient white light-emitting polymers from dual thermally activated delayed fluorescence chromophores for non-doped solution processed white electroluminescent devices. *Polym. Chem.* **2021**, *12*, 1030−1039.
57 Zhang, K.; Zhang, W.; Cao, Q.; Zhou, T.; Ge, F.; Xu, H.; Wang, J.; Ban, X.; Zhang, T. Turning the energy channel of side-chain TADF polymers by monomer optimization for high-efficiency solution-processed white OLEDs. *J. Lumin.* **2023**, *263*, 119966.
58 Zhao, J.; Liu, D.; Lu, Y.; Wu, Y.; Liu, Y.; Xu, S.; Su, S. J.; Cao, S. Solution-processable thermally activated delayed fluorescence red emitters poly(carbazole-fluorene) containing naphthalene imide units. *Polymer* **2023**, *285*, 126316.
59 Saikia, D.; Sarma, R. Performance improvement of organic light emitting diode using 4,4′-*N*,*N*′-dicarbazole-biphenyl (CBP) layer over fluorine-doped tin oxide (FTO) surface with doped light emitting region. *Pramana J. Phys.* **2018**, *91*, 65.
60 Wu, X.; Zeng, J.; Peng, X.; Liu, H.; Tang, B. Z.; Zhao, Z. Robust sky-blue aggregation-induced delayed fluorescence materials for high-performance top-emitting OLEDs and single emissive layer white OLEDs. *Chem. Eng. J.* **2023**, *451*, 138919.
61 Hu, J.; Li, Q.; Wang, X.; Shao, S.; Wang, L.; Jing, X.; Wang, F. Developing through-space charge transfer polymers as a general approach to realize full-color and white emission with thermally activated delayed fluorescence. *Angew. Chem. Int. Ed.* **2019**, *58*, 8405−8409.

https://doi.org/10.1007/s10118-026-3853-9